Renewable Energy 212 (2023) 803–817

Contents lists available at ScienceDirect

Renewable Energy

journal homepage: www.elsevier.com/locate/renene

Multi-decade high-resolution regional hindcasts for wave energy resource characterization in U.S. coastal waters

Zhaoqing Yang [a,b,*], Gabriel García Medina [a], Vincent S. Neary [c], Seongho Ahn [c], Levi Kilcher [d], Aidan Bharath [d]

[a] Coastal Sciences Division, Pacific Northwest National Laboratory, Seattle, WA, 98109, USA
[b] University of Washington, Department of Civil and Environmental Engineering, Seattle, WA, 98195, USA
[c] Sandia National Laboratories, Albuquerque, NM, 87185, USA
[d] National Renewable Energy Laboratory, Boulder, CO, 98109, USA

ARTICLE INFO

Keywords:
Wave energy
Resource characterization
High-resolution
Long-term simulations
Wave modeling
Nearshore

ABSTRACT

Long-term, high-resolution, regional wave hindcast datasets were generated using unstructured-grid Simulating WAves Nearshore (SWAN) models for the U.S. coastal waters to support nearshore wave energy development in the U.S. including those bordering U.S. territorial islands. The model domains resolved the entire U.S. exclusive economic zones, with a spatial resolution of approximately 200 m nearshore. The regional SWAN models were driven by the global WAVEWATCH III® model outputs and run for a 42-year period from 1979 to 2020. Extensive model validations were performed using buoy observations and altimeter data. Regional resource characterization was performed based on hindcast data points at 2 km from shore and along the 100 m isobath. Aggregations of wave resource parameters were produced, and spatial and seasonal variations were analyzed for all the regions. Wave resource metrics recommended by international standards, including a 3-h time series of six resource parameters, hourly frequency- and directionally resolved wave spectra at selected "virtual buoy" locations, and average-annual values of omni-directional wave power, significant wave height, and energy period are publicly disseminated through an Amazon Web Service and a Marine Energy Atlas web application tool to facilitate wave energy research and a wide range of coastal ocean applications.

1. Introduction

Wave energy is the most promising marine renewable energy source because of its vast resource and high predictability. As waves have high energy densities, relative to other renewable resources and can be forecasted reasonably well despite their short term and seasonal variability, they are a reliable renewable energy resource [1–5]. In the United States, wave energy resources make up approximately 80% of the ocean hydrokinetic energy resources (wave, ocean currents, and tidal currents) [6]. The global theoretical potential of wave energy is estimated 29,500 TWh per year [7], which is more than double the current global electricity demand of 13,400 TWh [8]. The theoretical wave energy along the edge of the continental shelf of the United States (U.S.) is estimated at 2640 TWh/year [9], approximately 65% of the annual electricity consumption 4054 TWh/year in U.S (https://www.energy.gov/sites/prod/files/2017/03/f34/qtr-2015-chapter4.pdf). The most abundant wave energy resources in the U.S. are found in coastal waters in the Pacific Ocean, e.g., the Aleutian trench, the West Coast, and the Hawaiian coast [9]. A variety of wave energy conversion (WEC) technologies designed to capture, absorb, and convert the energy transferred by ocean waves to electricity, or some other useful form of energy, are under development, but the industry is still in its pre-commercial phase, partially due to the lack of detailed information about wave climate and resource characteristics at the regional scale.

Wave energy resource characterization and assessment provide essential data and information to support WEC project siting, permitting, and development [10]. Significant efforts have been carried out to assess the wave resource at regional or nation-wide scales around the world based on wave hindcasts, including in the USA [11–13], Australia [14,15], European Atlantic Coast [16], India [17], China [18,19], Japan [20,21], France [22,23], Scotland [24,25], Portugal [26,27], Italy [28,29], Persian Gulf [30], and others. Some efforts have been carried out to assess the global wave resource using global hindcast datasets. Rusu and Rusu [31] estimated global wave power based on a 30-year ERA5

* Corresponding author. Coastal Sciences Division, Pacific Northwest National Laboratory, Seattle, WA, 98109, USA.
E-mail address: zhaoqing.yang@pnnl.gov (Z. Yang).

https://doi.org/10.1016/j.renene.2023.03.100
Received 26 December 2022; Received in revised form 21 March 2023; Accepted 22 March 2023
Available online 24 March 2023

database from 1989 to 2018. An assessment on global wave resource and inter-annual variability was conducted by Reguero, Losada [32] based on a long-term global ocean wave reanalysis dataset from 1948 to 2000. However, most of these resource assessments were at the reconnaissance level and lacked the spatial resolution needed for accurate characterization and assessment in the nearshore areas where initial WEC deployments are expected. The high-performance computing resources and storage required for multi-decade high-resolution model hindcasts with extensive coverage, and their costs, can be prohibitive. For example, the first U.S. nation-wide wave resource assessment, conducted by the Electric Power Research Institute, was based on a global-regional nested WAVEWATCHIII model with 4 arc minute (~5–7 km) resolution in the nearshore region [11]. Similarly, Australia's national wave energy resource assessment was based on a 35-year hindcast using the nest-grid modeling approach with 4 arc minute resolution nearshore. Alternatively, model resolutions in the nearshore areas can be further refined using multi-level nested grids. However, for a national-scale resource assessment. It is preferable to maintain model consistency in terms of model configurations and inputs, validation methods, and model output formats using the same modeling approach.

A joint effort, funded by the U.S. Department of Energy's Water Power Technologies Office, was carried out by Pacific Northwest National Laboratory (PNNL), Sandia National Laboratories (Sandia), and National Renewable Energy Laboratory (NREL) to generate and disseminate high-quality wave hindcast datasets to support wave resource characterization and assessment and coastal applications in U. S. coastal waters (https://openei.org/wiki/PRIMRE/Signature_Projects/Resource_Characterization). The overall objectives of the study were as follows: (1) generate long-term, high-resolution wave hindcasts that cover the entire U.S. Exclusive Economic Zone (EEZ), at sufficient resolution in the nearshore regions, for feasibility and design-level resource characterization and assessment; (2) improve model accuracy through extensive model validation and compute the IEC wave resource metrics [10]; and (3) develop and enhance data-sharing tools to disseminate the hindcast datasets and resource metrics through, an open-access web--based platform, the Marine Energy Atlas (https://maps.nrel.gov/marine-energy-atlas/), for spatial data on marine energy resources. Ultimately, the wave hindcasts will provide long-term, high-resolution datasets of wave energy resource attributes and wave conditions to advance the wave energy industry. The datasets will inform WEC design; help develop wave energy resource classification systems that facilitate regional energy planning; and help characterize opportunities, constraints, and risks to coastal engineering projects.

The structure of this paper is as follows. The methodologies, including model domain, model grids, and model configurations are described in Section 2, followed by model validation with buoy data and altimetry data in Section 3. Wave resource characterization at a regional scale is presented in Section 4. Hindcast data dissemination is described in Section 5, and conclusions are summarized in Section 6.

2. Methods

2.1. Study domains

As a nation-wide wave resource assessment, the study domains cover the entire U.S. EEZ, which extends up to 200 nautical miles (370 km) offshore and can be divided into eight regions: East Coast, Gulf of Mexico (GoM), Puerto Rico and U.S. Virgin Islands (PRUSVI), West Coast, Southern Alaska, Hawaii, U.S. Pacific Territories (USPT) (Fig. 1) (https://www.gc.noaa.gov/documents/2011/012711_gcil_maritime_eez_map.pdf). The area of each U.S. EEZ region, as well as the corresponding model grid points are presented in Table 1. The USPT (a combination of seven subregions) has the largest EEZ area of 3,328,925 km^2, followed by Southern Alaska with 2,836,000 km^2. The PRUSVI region has the smallest EEZ area—211,429 km^2. The total EEZ area covered by this study is 11,300,382 km^2, which includes most of the U.S. EEZ except for

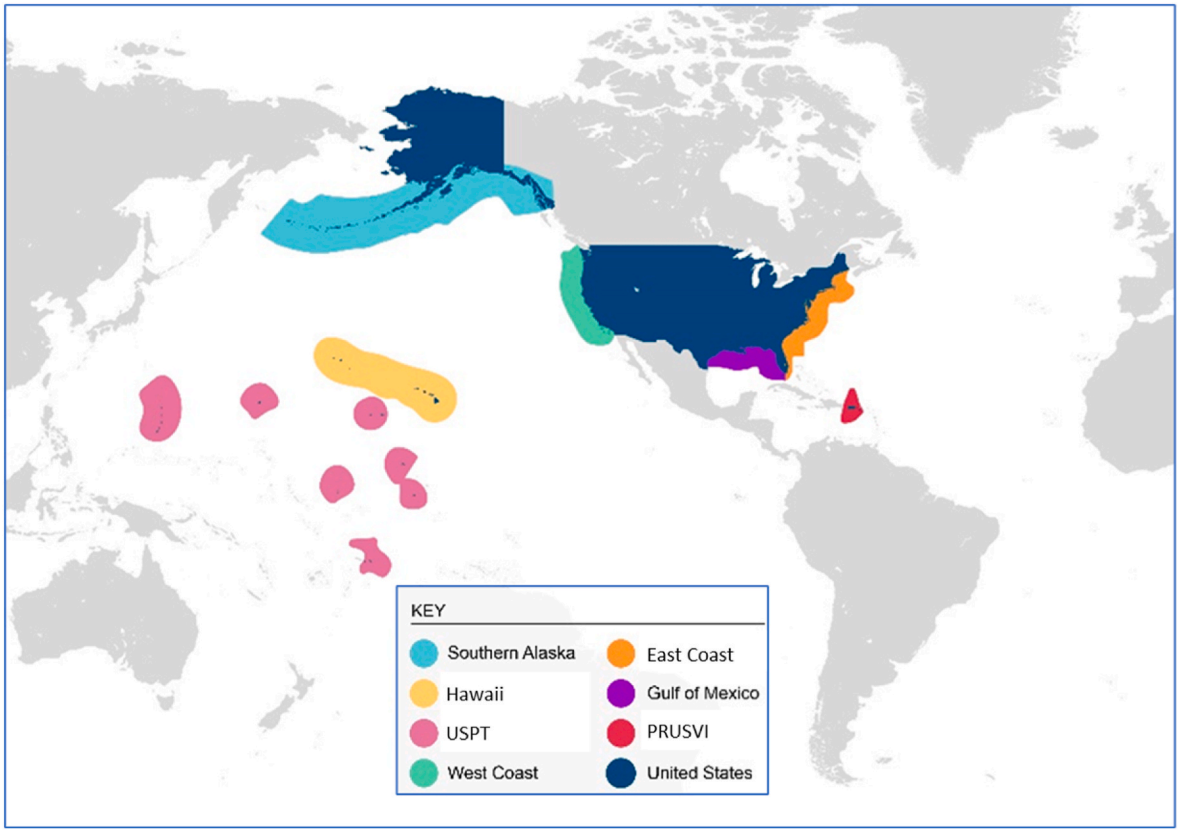

Fig. 1. U.S. EEZ regions corresponding to Table 1 for wave resource assessment.

Table 1
Areas of U.S. EEZ regions considered in this study and details of the models used.

Region	EEZ (km^2)	Model Grid Points[c]
West Coast	825,549	699,904
Southern Alaska	2,836,000[a]	3,894,283
Hawaii	2,474,884	1,696,188
U.S. Pacific Territories (USPT)	3,328,925[b]	1,470,061
East Coast	915,763	2,635,135
Gulf of Mexico (GoM)	707,832	3,351,881
Puerto Rico and U.S. Virgin Islands (PRUSVI)	211,429	1,304,756
Total	11,300,382	14,552,304

[a] The total area for the entire Alaska EEZ is 3,770,000 km^2.
[b] Commonwealth of Northern Mariana Islands, Guam, American Samoa, Jarvis Island, Johnston Atoll, Palmyra Atoll and Kingman Reef, Baker and Howland Islands, and Wake Island.
[c] Model grids cover larger areas than the EEZs, especially for the U.S. East Coast and GoM.

northern Alaska.

Note that the coverages of the EEZ areas are not exactly the same as the model domains that consider the effect of physical processes in each region. For example, the effect of sea ice was not considered in this current study. Therefore, the northern Alaska coast (north of the Aleutian Islands and Bristol Bay) was excluded from the model domain because the northern Bering Sea and the Arctic Coast are covered with sea ice most of the year and wave energy there is small [33,34]. In the Atlantic Ocean, model domains (East Coast, GoM, and PRUSVI) extend much farther out of the EEZ to the central ocean basin, and they account for the local growth of wind waves and swells [35,36]. More discussion of model domain configurations is provided in Section 2.3.

2.2. Wave models

Several widely used third-generation phase-averaged wave models simulate the ocean wave dynamics and account for all the physics of wave growth and dissipation in the ocean and shallow-water regions; they include WAM [37], WAVEWATCH III [38,39]. SWAN [40,41], TOMWAC [42] and MIKE-21 SM [43]. Over the past decade, unstructured-grid wave models have been developed rapidly and with the flexibility to account for the need for high resolution in the nearshore area and better representation of complex shorelines and computational efficiency in a large model domain.

The wave model used in this study is the unstructured-grid version of the Simulating Wave Nearshore (SWAN) Cycle III Version 41.10 [44]. SWAN solves the spectral action balance equation:

$$\frac{\partial N}{\partial t}+\frac{\partial c_x N}{\partial x}+\frac{\partial c_y N}{\partial y}+\frac{\partial c_\theta N}{\partial \theta}+\frac{\partial c_\sigma N}{\partial \sigma}=\frac{1}{\sigma}\left(S_{in}+S_{wc}+S_{nl4}+S_{bot}+S_{brk}\right) \quad (1)$$

where N is the wave action, c_x and c_y are the group velocity in the spatial domain based on linear wave theory, c_θ and c_σ are the propagation velocities in spectral domain, θ is the wave direction, and σ is the radian frequency of the waves. The right-hand side represents the sinks and sources of energy. S_{in} and S_{wc} are wind input and whitecapping; S_{nl} is the nonlinear quadruplet interactions; S_{bot} and S_{brk} are the dissipation due to bottom friction and depth-induced wave breaking, respectively. For the detailed definitions and descriptions of source terms, readers are referred to Refs. [45–48].

WAVEWATCH III global wave reanalysis developed by the U.S. National Oceanic and Atmospheric Administration (NOAA) was also used in this study to provide boundary conditions for all regional SWAN model hindcasts from 1979 to 2020 for a period of 42 years. The WAVEWATCH III global wave reanalysis has been thoroughly validated using in situ data and satellite-borne altimeters [49].

2.3. Model configurations

All regional SWAN models were forced by the NOAA global wave hindcast based on WAVEWATCH III at the open boundaries (see Section 2.2) and wind fields at the sea surface. Wind forcing comes from the Climate Forecasting System Reanalysis (CFSR) from January 1980 through March 2011 and from the Climate Forecast System (CFSv2) from April 2011 onward [50,51]. Wind was bilinearly interpolated from CFSR and CFSv2 into the model domains. Because of the availability of the different versions of wind forcing (CFSR and CFSv2), our wave hindcast study was also divided into two phases: Phase 1 covers the period from 1979 to 2010 and Phase 2 from 2011 to 2020. During Phase 1, the natural Gaussian grid was used as a source of the wind in the Atlantic, GoM, and Caribbean. The 0.5° reprojection was used as the wind source for the Pacific regions during Phase 1. Out of all models, the Hawaii model was the exception; it used a dynamically downscaled wind product from the University of Hawaii. The downscaling was done using Weather Research and Forecasting to a spatial resolution of 5 km and used CFSR as boundary conditions [52]. During Phase 2, all regions used the same CFSv2 0.2° grid as a source for wind interpolation. Although discrepancies exist between CFSR and CFSv2 in terms of model resolution and availability of data for assimilation, both models have been found to be suitable for wave hindcasting [53].

We strived to achieve a consistent model configuration, but some of the parameters had to be adjusted to account for local characteristics. In the case of the East Coast, the SWAN model domain was extended to the Central Atlantic. The large model domain resulted in a significant fetch for development of local waves and swells within the domain. Therefore, it was found, through a calibration analysis, that approximating the two-dimensional spectrum using a Gaussian distribution in directional space and JONSWAP in frequency space provided good results. These data were collected at the open boundary from bulk wave parameter output [36]. In the case of the Pacific domains, WAVEWATCH III was reimplemented to store spectral output at the SWAN open boundaries. There are two reasons for this distinction. The first is that the SWAN models do not extend much beyond the EEZ and thus the open boundaries have a larger effect on the waves within the domain. In addition, multimodal sea states are the norm in the Pacific Ocean. For example, in American Samoa waves generated in the Southern Ocean, the Northwest Pacific, and the tropical Pacific can all reach the territory simultaneously, thus requiring a frequency and directionally resolved spectral characterization of the boundary conditions [66]. WAVEWATCH III was reimplemented following the same approach used in the NOAA reanalysis with the distinction of two new meshes being developed for the tropical Pacific at 10 and 4 arc minute resolutions; these resolutions were consistent across the rest of the domains.

SWAN default formulations for third-generation physics were initially used. A calibration procedure was performed on the East Coast to determine the adequate model coefficients. Except for Southern Alaska, all models included triad interactions following Edelberky (1996) [54]. The West Coast model described in Refs. [55,56] initially did not include triad interactions but was executed again including triad interactions for completeness. In addition, the model domain was extended to cover the EEZ and is described in Ref. [57].

The frequency ranges in all regions were determined via convergence analysis, which resulted in varying low- and high-frequency cutoffs. However, a common range between 0.04 and 0.5 Hz was resolved in the models. The Pacific Ocean models had a lower minimum frequency to account for the transpacific swells that generally have longer wave periods. In contrast, significant local wave generation activity occurs in the GoM and PRUSVI, and thus a higher frequency cutoff was used to accurately account for these waves. In addition, the base directional resolution considered was 15°. However, sensitivity analyses were performed in all regions to ensure model convergence and to mitigate the Garden Sprinkler Effect (GSE). A directional resolution of 5° was found to be necessary around Alaska, Hawaii, and the USPT to mitigate this

effect, while the resolution needed to be increased to 10° in the PRUSVI. GSE is more evident with swell propagation, which varies by location.

In the SWAN model solution, there is a close interplay between the number of iterations in the Gauss Siedel algorithm and the time step. In essence they are nested loops in the model solution. These two parameters have a large influence on the computing time, and it was desirable to minimize the number of iterations and maximize the time step. SWAN in its unstructured solution is not subjected to the Courant–Friedrichs–Lewy criterion because the solution method is implicit [58]. A convergence analysis was carried out in all regions to determine the least computational effort needed to avoid solution deterioration. Swells traveling across the mesh, the number of sub-domains used to solve the equations using the Message Passing Interface, and the physical size of the mesh all influence these characteristics. Therefore, this parameter is expected to vary by model. In the case of the USPT, except for the Commonwealth of the Northern Mariana Islands and the U.S. Territory of Guam (CNMI-Guam) and American Samoa, the maximum number of iterations allowed was five, but over 99% of the time the model converged in two iterations. Because the models were smaller, there was no need to limit the number of iterations to decrease runtime. Model configurations for all the regions are summarized in Table 2.

2.4. Model grids and resolutions

The WAVEWATCH III global hindcast reanalysis employed a three-level nested-grid approach with a global grid resolution (Level-1) of 0.5° and regional nested-grid resolutions (Level-2 and -3) of 10 and 4 arc minutes, respectively. However, the WAVEWATCH III regional grids were found to not fully cover the EEZ regions in both the Southern Alaska and West Coast regions, and they only cover a small portion of the Hawaii region. There are no regional nested grids for the USPT. Therefore, in the Pacific Ocean the extents of the 10 and 4 arc minute WAVEWATCH III models off Southern Alaska and the West Coast were extended beyond the U.S. EEZ. In the Central Pacific, new WAVEWATCH III 10 and 4 arc minute models were developed to cover all USPT and Hawaii.

Separate SWAN models were developed for each region to incorporate the local conditions in the modeling system. In Hawaii, the mesh size was depth dependent to account for refraction due to sea mounts that do not have surface expression but are shallow enough to refract waves. The model mesh has a resolution of 200 m for waters less than 500 m deep and relaxes to match the boundary resolution of 5 km. This same approach was taken in the rest of the USPT. The mesh around Southern Alaska was constrained to 300 m or finer within 30 km from shore. This was done to accurately model the swell exchanges between the North Pacific and the Bering Sea between the Aleutian Islands. The West Coast region has very narrow continental shelf, comparing to other regions. Instead of using a depth-dependent mesh generation method, a simple approach was taken to specify the mesh resolution in the range of 200–350 m in the nearshore areas.

The GoM and PRUSVI models were run on the same mesh, taking advantage of the unstructured-grid feature of SWAN. The model resolution in the nearshore region was specified as being approximately 200 m and gradually increased to 4000–5000 m near the U.S. EEZ and maintained the same outside EEZ for computational efficiency.

The total computational meshes for all the regions have more than 14.5 million grid points (nodes). Model grid points for each model domain are listed in Table 1. The total number of model grid points is proportional to the size of the model domain and to the complexity of the shorelines and number of islands where high model resolution is required. Examples of model meshes for the Hawaii, Southerm Alaska, and East Coast regions are shown in Fig. 2.

3. Model validation

Model validation is a critical step in understanding the accuracy of the models, sources of the errors, and the associated physical processes, before applying the wave hindcast datasets to resource characterization and assessment. In this study, model validation was conducted using two different methods based on the types of measurement data. The first method is the spectral wave buoy data method, which can be used to derive the six IEC resource parameters at buoy locations. The second is the altimetry data method, and only significant wave height was compared with altimetry data along all the satellite track locations where altimetry data were used to derive the significant wave height.

Model simulations for all the regions were conducted for a 42-year period from 1979 to 2020. Model runs were executed in three national labs' high-performance computing facilities: Constance at PNNL, Chama and Skybridge at Sandia, and Eagle at NREL. A summary of the model validation with wave buoy data is provided in Section 3.2. Model validation using altimetry data is reported in Section 3.3.

Table 2
Regional model configurations.

Parameter	Southern Alaska	East Coast	PRUSVI	GoM	Hawaii	USPT	West Coast
Wind temporal resolution	1 h						
Wind spatial resolution	Phase1: 0.50°Phase2: 0.20°	Phase1: 0.32° Phase2: 0.20°			Phase1: 0.05° Phase2: 0.20°	Phase1: 0.50° Phase2: 0.20°	
Spectral boundary conditions	Two-dimensional Spectrum						
Wind input	Janssen (1991) [59]; Cavaleri and Malanotte-Rizzoli (1981) [47]						
Quadruplet interactions	Hasselmann et al. (1985) [45]						
Whitecapping	Janssen (1991) [59]						
Triad interactions	No	Edelberky (1996) [54]					
Depth-induced breaking	Battjes and Janssen (1978) [46]						
Bottom friction	JONSWAP (1973) [60]						
Sea ice	Considered in WAVEWATCH III forcing [39]						
Minimum spatial resolution	200 m in nearshore areas						
Number of frequencies	29	28	28	28	31	34	29
Frequency range (Hz)	0.035–0.505	0.040–0.520	0.040–1.0	0.040–1.0	0.030–0.505	0.030–0.697	0.035–0.505
Directional resolution	5°	15°	10°	10°	5°	5°	10°
Time step (min)	10	10	3	3	2	3–5	5
Iterations	2	1	3	3	5	5	3

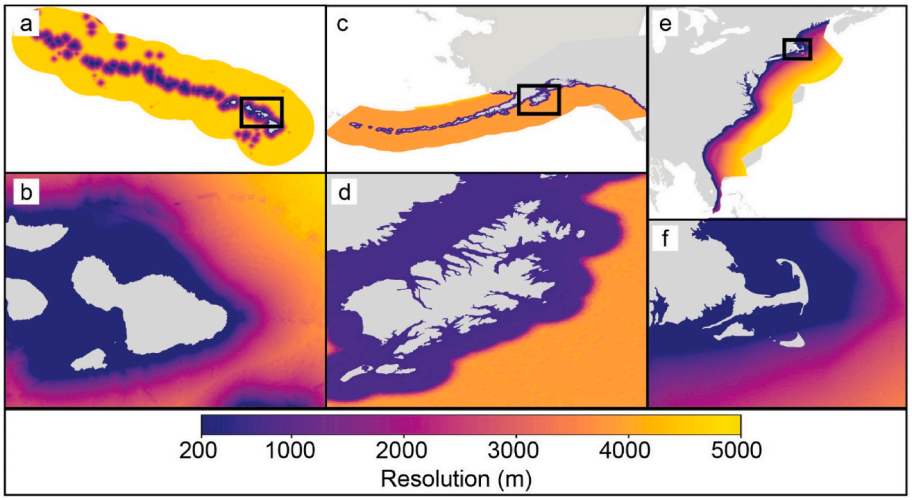

Fig. 2. Examples of SWAN model domains and mesh resolutions for Hawaii (a, b); Southern Alaska (c, d), and East Coast (e, f) regions.

3.1. Wave resource parameters and model performance metrics

As recommended by IEC-TS 62600–101 [10], six resource parameters should be calculated and analyzed for any wave energy resource characterization and assessment: omnidirectional wave power, significant wave height, wave energy period, spectral width, the direction of maximum directionally resolved wave power, and the directionality coefficient [10]. However, by default, SWAN v41.10 does not compute omnidirectional wave power, the directionality coefficient, and the direction of maximum directionally resolved wave power, although some parameters, such as total wave power, can be calculated based on SWAN outputs [61]. This capability was added to SWAN v41.10 to calculate and store the six IEC resource parameters at each computational grid point [36,55]. The definitions of the six IEC wave resource parameters are described below.

Omnidirectional wave power ($J\,[W/m]$) is the flux of energy through a unit circle and describes the density of power:

$$J = \rho g \sum_{i,j} c_{g,i} S_{ij} \Delta f_i \Delta \theta_j \tag{2}$$

where ρ is the water density, g is the acceleration of gravity, c_g is the group velocity, S_{ij} is the directionally and frequency resolved variance spectrum, f is the discrete frequency, and θ is the discrete wave direction.

The significant wave height provides a characteristic wave height of the sea state and is defined as follows:

$$H_{m0} = 4.004\sqrt{m_0} \tag{3}$$

where m_0 is the zeroth spectral moment. Spectral moments are computed from the variance spectrum via:

$$m_n = \sum_i f_i^n \left(\sum_j S_{ij} \Delta\theta_j \right) \Delta f_i \tag{4}$$

Following linear wave theory, $H_{m0}\,[m]$ is directly proportional to the total energy of the sea state:

$$E = \frac{1}{16} \rho g (H_{m0})^2. \tag{5}$$

The energy period ($T_e\,[s]$) is presented as a characteristic wave period:

$$T_e = \frac{m_{-1}}{m_0} \tag{6}$$

where the spectral moments are computed following Eq. (4). The spectral width (ε_0) characterizes the spread of the energy in frequency space:

$$\varepsilon_0 = \sqrt{\frac{m_{-0} m_{-2}}{m_{-1}^2} - 1} \tag{7}$$

The directional characteristics of the sea state can be described by the directionally resolved wave power:

$$J_\theta = \rho g \sum_{i,j} c_{g,i} S_{ij} \Delta f_i \Delta \theta_j \cos(\theta - \theta_j) \delta \begin{cases} \delta = 1, \cos(\theta - \theta_j) \geq 0 \\ \delta = 0, \cos(\theta - \theta_j) < 0 \end{cases} \tag{8}$$

where only the wave power crossing a vertical plane perpendicular to a direction θ is accounted for. The direction of maximum directionally resolved wave power θ_{Jmax} is the direction that maximizes J_θ. The directionality coefficient (d) characterizes the directional spread of wave power:

$$d = \frac{J_{\theta_{Jmax}}}{J} \tag{9}$$

where $J_{\theta_{Jmax}}[W/m]$ is the wave power at θ_{Jmax}. The six parameters defined above provide a comprehensive description of the sea state adequate for a reconnaissance study.

The most commonly used error metrics for evaluating the model performance for non-directional resource parameters are the root-mean-square-error (RMSE), scatter index (SI), bias (b), and the linear correlation coefficient (R):

$$RMSE = \sqrt{\frac{\sum_{i=1}^{N} (P_i - M_i)^2}{N}} \tag{10}$$

$$SI = \frac{RMSE}{\overline{M}} \tag{11}$$

$$bias = \frac{1}{N} \sum_{i=1}^{N} P_i - M_i \tag{12}$$

$$\mathrm{R} = \frac{\sum_{i=1}^{N} (P_i - \overline{P})(M_i - \overline{M})}{\sqrt{\left[\sum_{i=1}^{N} (P_i - \overline{P})^2\right] \left[\sum_{i=1}^{N} (M_i - \overline{M})^2\right]}} \tag{13}$$

where N is the number of measurements, M_i is the measured data, P_i is the predicted results, and overlines represent the time average. To evaluate the model performance for directional resource parameters, i.e., direction of maximum directionally resolved wave power and directionality coefficient, the angular bias (b_θ) [62] and the circular correlation (R_θ) were used following the Hanson et al. [63] method:

$$bias_\theta = \tan^{-1}\frac{\sum_{i=1}^{N}\sin|P_i - M_i|}{\sum_{i=1}^{N}\cos|P_i - M_i|} \quad (14)$$

$$R_\theta = \frac{\sum_{i=1}^{N}\sin(P_i - \overline{P})\sin(M_i - \overline{M})}{\sqrt{\left(\sum_{i=1}^{N}[\sin(P_i - \overline{P})]^2\right)\left(\sum_{i=1}^{N}[\sin(M_i - \overline{M})]^2\right)}} \quad (15)$$

3.2. Model validation with buoy data

All the regional models have been validated with wave buoy data from the NOAA National Data Buoy Center (NDBC), the Coastal Data Information Program (CDIP), Fisheries and Ocean Canada, and Pacific Islands Ocean Observing System (PacIOOS). Model results were validated not only for six IEC resource parameters but also for wave spectral characteristics. Detailed model validation results and discussion were reported in previous studies [33,35,36,55,64–67]. A summary of the model validation for the six regional IEC parameters for all the regions is provided in this section.

All the buoys within the SWAN model domains for which data records exist for the period from 1979 to 2020 were considered in the model validation efforts. A total of 110 buoys were used for the model validation. The West Coast region has the most buoys (42), followed by Southern Alaska (23) and Hawaii (22). PRUSVI and USPT have the fewest—only four buoys in each region. Fig. 3 shows the distributions of buoys color-coded by region.

The regional averaged error statistics for the six IEC resource parameters are shown in Table 3 through 5. Note that for the directional parameters, i.e., direction of maximum directionally resolved wave power, only bias and the linear correlation coefficient were calculated. For significant wave height H_{m0}, the RMSEs are in the range of 0.24–0.48 m (Table 3), the highest being in the Southern Alaska and West Coast regions where waves are strong. The scatter index, a normalized error parameter (Eq. (11)), ranges from 0.17 to 0.28 (Table 3), and the highest occurred in the East Coast region where wave heights are generally low but are subject to the impact of extreme waves induced by tropical cyclones during the hurricane season (summer and fall). The biases for the simulated wave heights are small and positive (except for PRUSVI), indicating the models are slightly overpredicting the significant wave heights at the regional scale. The linear correlations are also very good, all above 0.92, except for the East Coast region that has a value of 0.88 (Table 3). The trends in the error statistics for the omnidirectional wave power are similar to those for significant wave height but have larger values (Table 3) because the wave energy is proportional to the square of the significant wave height (Eq. (5)). The scatter indexes for the East Coast and GoM regions are noticeably greater than those for other regions because the average wave power in those two regions is small (see Section 4.2). Waves in these regions propagate over strong ocean currents and eddy systems, such as Florida Current and Gulf Stream. However, the present models did not consider wave-current interaction and wave dissipations associated with it, which may contribute to the error in simulating high-frequency waves that dominate the wave climate in areas with strong currents.

The RMSE for the energy period varies from 0.70 to 1.22 for all regions (Table 4). In general, the RMSEs show larger values in the Southern Alaska, West Coast, and Hawaii regions, likely because wave periods are much longer than the those in other regions, as indicated by the scatter index, which is below 0.18 for all the regions. The biases for the simulated wave energy period are mostly positive, indicating the models overpredicted the energy period, especially in the large regions like Southern Alaska, the West Coast, Hawaii, and the East Coast. However, the maximum bias is only 0.66 (in Hawaii), which showed the regional models accurately simulated the wave period, as indicated by the high linear correlation coefficients (Table 4). The RMSE, scatter index, and bias for the spectral width are generally small (Table 4). However, the linear correlation coefficients for the Southern Alaska, East Coast, and GoM regions are relatively low, likely due to model capability in capturing the wide spread of energy in the frequency domain under extreme sea states. The accuracy of the simulated ε_0 is

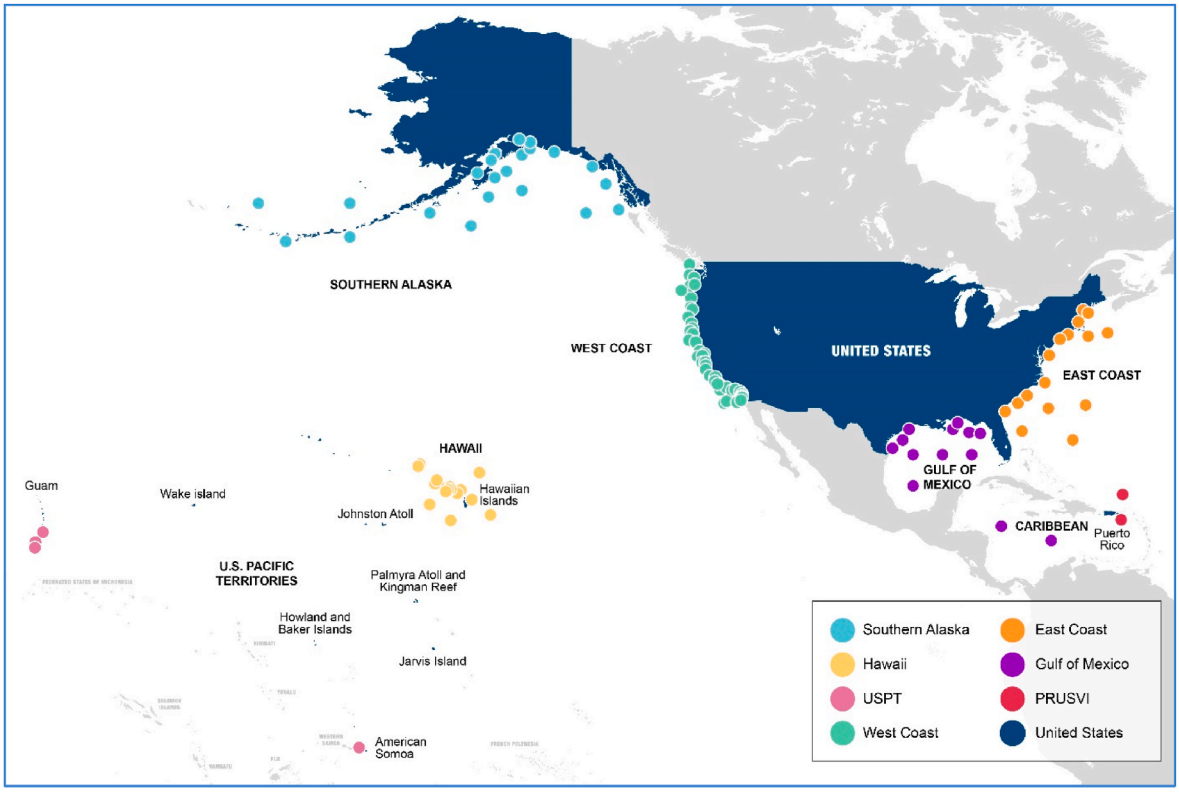

Fig. 3. Buoy locations for model validations in the Southern Alaska, Hawaii, USPT, West Coast, East Coast, GoM, and PRUSVI regions.

Table 3
Forty-two-year regional averaged error statistics for significant wave height and omnidirectional wave power.

		H_{m0} (m)				J (kW/m)			
Region	Buoy #	RMSE	SI	bias	R	RMSE	SI	bias	R
West Coast	46	0.40	0.22	0.16	0.93	13.5	0.65	4.0	0.92
Southern Alaska	23	0.48	0.21	0.10	0.95	22.8	0.75	7.7	0.91
Hawaii	22	0.32	0.17	0.04	0.92	11.0	0.61	2.0	0.88
USPT	4	0.27	0.16	−0.04	0.92	8.0	0.61	−0.25	0.82
East Coast	17	0.39	0.28	0.11	0.88	10.51	1.05	2.06	0.83
GoM	11	0.25	0.21	0.01	0.93	5.22	1.15	0.33	0.90
PRUSVI	4	0.24	0.18	0.03	0.92	5.12	0.71	1.19	0.88

Table 4
Forty-two-year regional averaged error statistics for energy period and spectral width.

	T_e (s)				ε_0			
Region	RMSE	SI	Bias	R	RMSE	SI	bias	R
West Coast	1.19	0.13	0.53	0.85	0.07	0.19	−0.01	0.73
Southern Alaska	1.22	0.16	0.61	0.84	0.10	0.29	0.02	0.54
Hawaii	1.21	0.15	0.66	0.86	0.07	0.18	−0.01	0.67
USPT	0.72	0.09	0.28	0.87	0.05	0.14	−0.01	0.68
East Coast	1.15	0.18	0.58	0.75	0.08	0.25	0.02	0.47
GoM	0.74	0.14	−0.05	0.82	0.09	0.30	0.03	0.51
PRUSVI	0.70	0.12	0.08	0.83	0.07	0.20	0.03	0.59

Table 5
Forty-two-year regional averaged error statistics for direction of maximum directionally resolved wave power and directionality coefficient.

	θ_{Jmax} (deg)		d			
Region	bias	R	RMSE	SI	bias	R
West Coast	11.0	0.88	0.09	0.11	0.04	0.73
Southern Alaska	17.3	0.73	0.15	0.21	0.07	0.46
Hawaii	8.8	0.87	0.10	0.14	0.01	0.63
USPT	9.0	0.88	0.08	0.10	0.04	0.86
East Coast	4.37	0.59	0.16	0.22	0.10	0.32
GoM	−0.77	0.89	0.11	0.12	0.05	0.62
PRUSVI	0.60	0.89	0.08	0.10	0.02	0.67

relatively low compared to other parameters as ε_0 is a highly non-linear function of the spectral moments. This error is more pronounced in modeling high-frequency wave climates, e.g., in the GoM, where the small error in high-frequency spectrum bands causes substantial changes in ε_0 calculation.

The error statistics (bias and R) for the direction of maximum directionally resolved wave power showed the model results are overall in good agreement with the data (Table 5). The absolute values of the biases are range from 0.66 deg in the PRUSVI region to 17.3 deg in the Southern Alaska region. The linear correlation coefficients are close to 0.9 except in the Southern Alaska (0.73) and East Coast (0.59) regions, which is again likely due to the challenge of simulating wave directions in areas of active wave growth and under extreme weather conditions. The directionality coefficient, a normalized parameter that relates to θ_{Jmax} and characterizes the directional spread of the energy distribution, showed good errors in RMSE, SI, and bias. However, the linear correlation coefficients were generally low.

3.3. Validation with altimetry data

Satellite-borne radar altimeters have provided near continuous significant wave height estimates since 1985, starting with the GEOdetic SATellite (GEOSAT) mission. Throughout the hindcast period of 1979–2020, a total of 14 missions provided data in the study regions. The mission names and timelines are shown in Fig. 4. These altimetry-based data are valuable because they can be used to evaluate spatial patterns of model performance, which is currently not possible with in situ measurements because doing so would require very dense wave buoy arrays. In addition, these altimeters provide total coverage in the study region. This is critical because five of the seven Pacific Island territories do not have in situ measurements during the study period. Furthermore, other regions are significantly subsampled; for example, there is only one buoy deployed in American Samoa and three buoys in the southern Mariana Islands. This dataset has two main limitations that must be acknowledged. First, the time interval between measurements is generally long, on the order of multiple days. Second, the on-board radar altimeters only provide significant wave height estimates. However, the agreement between altimeter estimates and in situ measurements has been found to be very high [1,68]. Despite these shortcomings, this dataset is still a very valuable source of data for model validation, particularly in regions where no in-situ measurements occur, and it has been used in previous wave resource assessments [69].

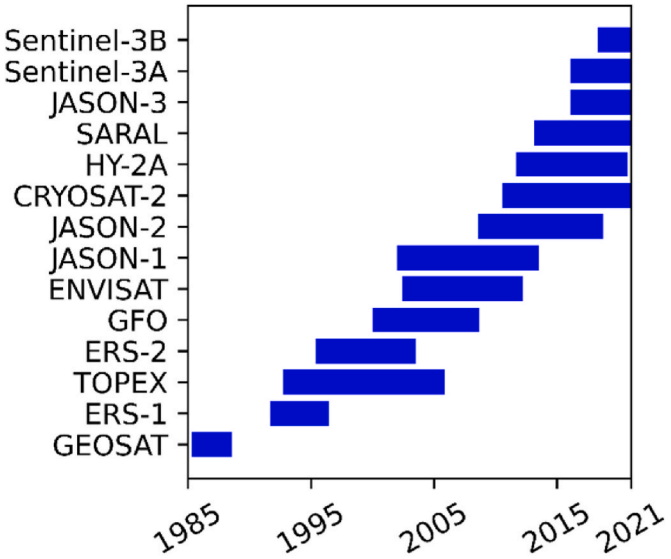

Fig. 4. Missions that provide publicly available significant wave height used for model validation.

Significant wave height is measured by actively emitting microwaves

in the Ku band (13–17 GHz) in all missions except Satellite with ARgos and ALtika (SARAL) mission, which used a Ka band at 35.75 GHz. The sea surface variance is estimated from the shape of the waveform returns [70]. Data were downloaded from the Australian Ocean Data Network portal (https://portal.aodn.org.au/), which has a consistent database because data were reprocessed for all missions using a consistent algorithm (the technical details can be found in Ref. [1]). To facilitate model-data comparisons the data are binned over a 0.20°grid. These bins measure 22.2 km in the meridional direction and vary from 22.2 km at the equator to 11.1 km at 60°N in the zonal direction. Each bin must contain at least 200 model-data pairs to be considered for use in model validation.

The spatial distribution of RMSE using altimetry data is shown in Fig. 5. Overall, Southern Alaska has the maximum error (up to 0.75 m) compared to other regions, followed by the West Coast, East Coast, and northern Hawaii regions. The Pacific coast of the Aleutian archipelago has the highest 90th percentile waves in the U.S. EEZ [71]; thus, higher RMSEs, which are dimensional, can be expected. Simulated significant wave heights are in good agreement with altimetry data in the USPT, GoM, and PRUSVI regions (Fig. 5). In the East Coast, the offshore sites with relatively large error (red stream along the East Coast in Fig. 5) overlay with the Gulf Stream, demonstrating the influence of ocean currents on the wave modeling in the East Coast region.

Error statistics for significant wave height averaged over the entire EEZ regions are shown in Table 6. The RMSE ranges from 0.33 m in the USPT to 0.75 m in Southern Alaska. The trend and values of error statistics for the significant wave height using altimetry data (Table 6) are consistent with those shown in Table 3 using wave buoy data, which confirms the model validation methodologies using both observation datasets are correct and the regional models are capable of accurately simulating wave dynamics in the U.S. coastal waters using the multi-scale, multi-resolution approach.

4. Regional resource characterization

The six IEC resource parameters were outputted at every grid point of the model domain and at 3-h intervals for the 42-year period. Once all six IEC resource parameters are produced for all regions, resource characterization can be performed at the regional scale by calculating the aggregated resource parameters and analyzing the regional and temporal variabilities of wave energy, following the methodologies recommended.

Table 6
Error statistics for significant wave height for different regions using altimetry data.

Region	RMSE (m)	SI	bias (m)	R
West Coast	0.48	0.20	0.21	0.92
Southern Alaska	0.74	0.28	0.10	0.87
Hawaii	0.39	0.17	0.09	0.88
USPT	0.33	0.16	−0.01	0.85
East Coast	0.49	0.29	0.17	0.88
GoM	0.33	0.31	0.03	0.87
PRUSVI	0.34	0.23	0.11	0.82

4.1. Aggregation of wave resource parameters

As recommended by IEC-TS 62600–101, aggregated wave resource parameters were calculated for each region. Because the nearshore area is the most promising area for harvesting wave energy, we calculated the aggregated wave resource parameters in the nearshore for all the regions. We characterized wave resources for each region at locations based on two factors: the distance from the shore and the water depth. Data were collected at points 2 km from shore and at the 100 m isobath around all the coasts. Model results were extracted at a spatial resolution (distance between two data stations) of 1 km and at 3-h intervals for the statistics analysis. Two kilometers from shore was chosen, rather arbitrarily, to represent the practical distance for shore-connected devices. The 100 m isobath was selected to complement the analysis and explore the diversity of sites around the U.S.

Fig. 6a shows the distributions of water depth for data points at 2 km from the shore and the distance from shore for data points along the 100 m isobath. Clearly, at the 2 km distance from shore, nearly 100% of the data points are within 50 m water depth in the East Coast and GoM regions because of the broad continental shelf. In contrast, most of the stations in the USPT and Hawaii regions are in waters deeper than 500 m (Fig. 6a). This is because the insular shelves are much narrower than the continental shelf. Stations at 2 km offshore in the West Coast and Southern Alaska regions are distributed within 200 m water depth and the largest fraction of them are within 50 m (Fig. 6a). Stations in Hawaii spread out across a wide range of water depths up to 1000 m deep, but most are evenly distributed in areas shallower than 200 m depth

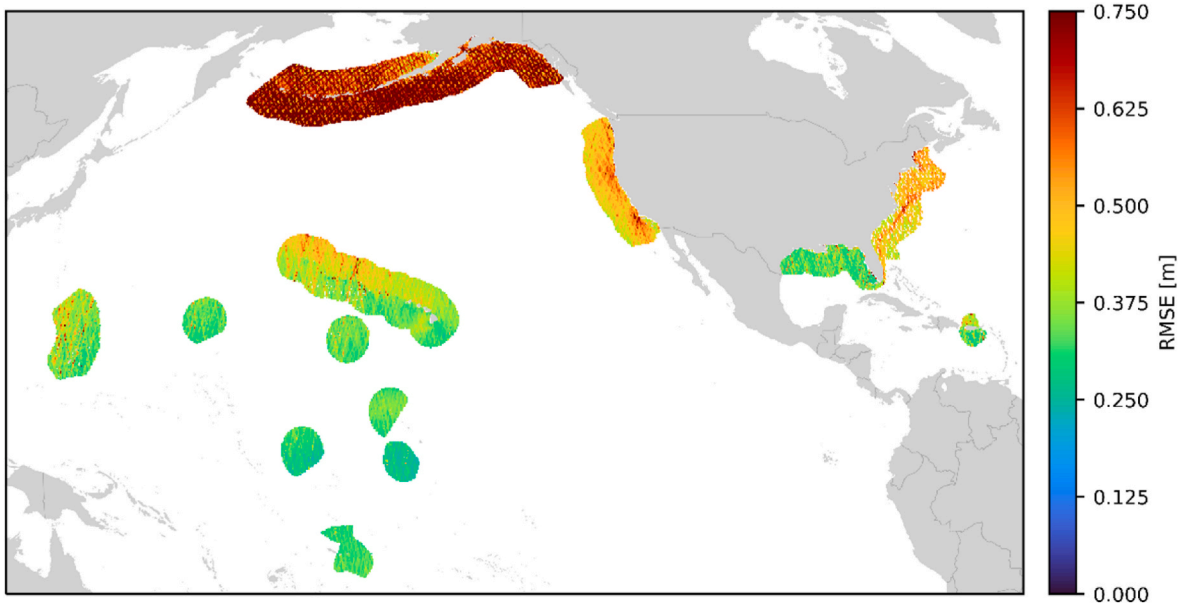

Fig. 5. Distributions of RMSE of simulated significant wave height in U.S. EEZ using altimetry data.

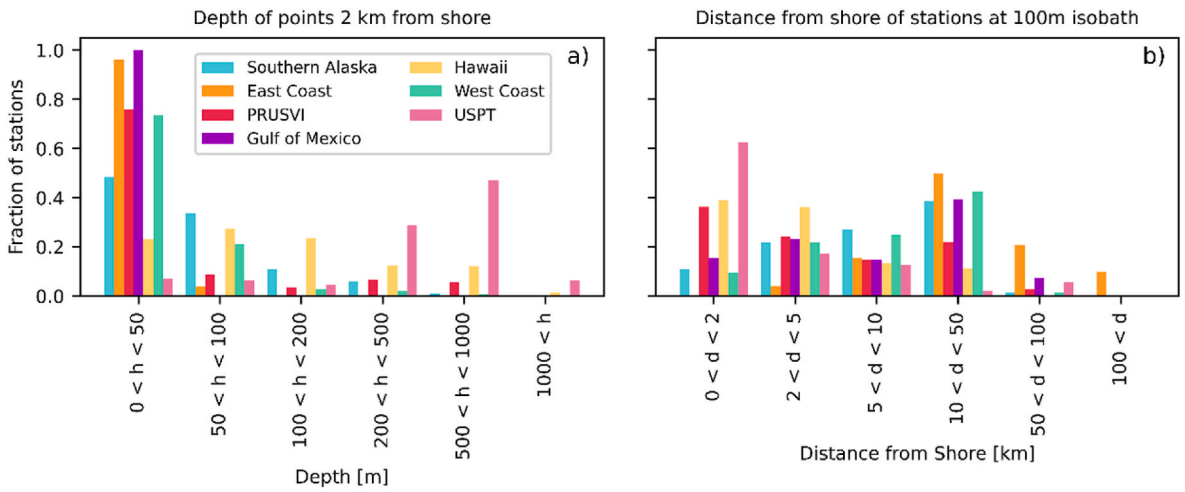

Fig. 6. Distribution of data points used in aggregated statistical analysis of wave resource parameters (a) as a function of water depth at 2 km distance offshore and (b) as a function of distance from shore along the 100 m isobath.

(Fig. 6a).

On the other hand, most stations (>60%) along the 100 m isobath in the USPT region are less than 2 km from shore (Fig. 6b). In the East Coast region, most of the stations along the 100 m isobath are more than 10 km from shore, and more than 50% stations are located in the range of 10–50 km offshore (Fig. 6b). In the West Coast, Southern Alaska, and GoM regions, stations along the 100 m isobath showed an increasing trend in distance offshore—most of them are located between 10 and 50 km from shore (Fig. 6b). In contrast, stations in the Hawaii and PRUSVI regions showed a decreasing trend in distance offshore; the largest fraction of stations is located within 2 km from shore (Fig. 6b).

The approach of combining two sets of samples based on two important factors (water depth and distance from shore) can provide valuable insight when evaluating and comparing the resource across regions. However, the specific values (100 m water depth and 2 km distance from shore) chosen in this study only serve as examples for users who want to perform similar analyses with different distances from shore or water depths that are better suited for their applications in the future. This high-resolution dataset allows users to assess the resource at a given depth even if it is located very close to shore.

Aggregated values for the five IEC resource parameters were calculated for each region at 2 km from shore and at the 100 m water depth are shown in Tables 7 and 8, respectively. The direction of maximum directionally resolved wave power was not considered because it is meaningless to average the directions. Compared with J, H_{m0} and T_e, the Pacific (Southern Alaska, Hawaii, West Coast, and USPT regions) is more energetic than the Atlantic (East Coast and PRUSVI regions) at 2 km from shore, because the Atlantic faces the direction of the westerlies and is in the path of intense extratropical storms [72]. In the Pacific, the overall most energetic region is the West Coast region, which has an average J of 16.9 (kW/m), an H_{m0} of 1.4 m and a T_e of 9.4 s. The Pacific-facing coast of Southern Alaska is more energetic than the West Coast, but the Bering Sea-facing shores are also aggregated in this analysis and are significantly less energetic [33]. These aggregate statistics provide guidance on the expected energy production if wave energy converters are spread evenly along the coast at 2 km from shore. The USPT region has higher omnidirectional wave power at 2 km from shore than the Southern Alaska region. This is mostly driven by the relatively small size of the islands, and they cast little shadow on the wave energy resource [64], which implies that a significant amount of power can be found close to shore and in multiple directions. Note that the average values of the resource parameters in the USPT region do not equal the means of the values for the subregions because they are weighted by the number of stations around each subregion. In the East Coast region, the average omnidirectional wave power increases with distance from shore [35]. The offshore along the East Coast is more exposed to swells generated by nor'easter and Bermuda High pressure system, while the nearshore is more dominated by local wind seas [71, 73]. The GoM region has the lowest wave resource at 2 km from shore compared to the rest of the regions, with an average J of 1.1 (kW/m), an H_{m0} of 0.4 m, and a T_e of 3.5 s. This is because the GoM is a semi-enclosed basin and therefore is fetch limited and dominated by local wind-seas.

As shown in Table 8, a significant amount of the wave energy resources in the East Coast region are located farther offshore because the

Table 7
Aggregated statistics for wave resource parameters 2 km offshore.

Region	J(kW/m)	H_{m0}(m)	T_e(s)	ε_0-	d-
West Coast	16.9	1.4	9.4	0.39	0.89
Southern Alaska	12.7	1.3	7.0	0.45	0.85
Hawaii	11.6	1.4	8.6	0.41	0.78
USPT	13.0	1.6	8.2	0.37	0.77
American Samoa	14.6	1.7	9.2	0.39	0.70
Baker and Howland Islands	15.0	1.8	9.0	0.38	0.65
CNMI-Guam	11.8	1.5	7.8	0.35	0.81
Jarvis Island	15.7	1.9	8.9	0.41	0.63
Johnston Atoll	13.4	1.6	8.8	0.45	0.78
Palmyra Atoll and Kingman Reef	17.6	1.9	8.7	0.41	0.62
Wake Island	17.8	1.9	8.5	0.34	0.75
East Coast	3.8	0.8	6.4	0.38	0.90
GoM	1.1	0.4	3.5	0.40	0.89
PRUSVI	5.4	1.1	6.5	0.40	0.86

Table 8
Aggregated statistics for wave resource parameters along the 100 m isobath.

Region	J(kW/m)	H_{m0}(m)	T_e(s)	ε_0-	d-
West Coast	33.6	2.2	9.8	0.34	0.85
Southern Alaska	21.5	1.8	7.7	0.40	0.81
Hawaii	12.6	1.5	8.5	0.41	0.76
USPT	11.6	1.5	8.1	0.38	0.78
American Samoa	14.3	1.7	9.1	0.38	0.72
Baker and Howland Islands	10.6	1.5	8.7	0.39	0.73
CNMI-Guam	7.6	1.2	7.4	0.36	0.86
Jarvis Island	11.6	1.6	8.5	0.43	0.72
Johnston Atoll	18.9	2.0	8.4	0.40	0.71
Palmyra Atoll and Kingman Reef	18.7	2.0	8.5	0.41	0.60
Wake Island	10.3	1.4	7.9	0.37	0.84
East Coast	14.5	1.7	6.9	0.33	0.79
GoM	4.8	1.1	4.9	0.32	0.82
PRUSVI	7.1	1.2	6.7	0.38	0.86

energy is driven by nor'easter and Bermuda High pressure swells as mentioned above. The 100 m isobath on the East Coast is much farther from shore (5 km–100 km, see Fig. 6b) than in the rest of the regions, which also allows an extended fetch for continuous wind-wave growth beyond the 2 km distance from shore. Therefore, the average wave power in the East Coast region increases from 3.8 at the 2 km offshore to 14.5 kW/m along the 100 m isobath, which is comparable to the wave power in the Hawaii and USPT regions (Table 8). In addition, waves traveling toward shore have lost less energy to bottom friction at the 100 m isobath stations because of deep water. Wave resources in the West Coast and Southern Alaska regions at stations along the 100 m isobath also increase compared to those at 2 km from shore (Table 8), because most of the stations along the 100 m isobath are farther offshore than 2 km (Fig. 6b) and the waves are less dissipated before approaching to the shore. The differences in wave power between 2 km from shore and along the 100 m isobath are less significant around Hawaii and the USPT (Tables 7 and 8), because of the narrow insular shelf discussed previously.

4.2. Regional variability of wave resource

Regional distributions of 42-year averages of significant wave height, omnidirectional wave power, and energy period in all of the U.S. EEZ domains are shown in Fig. 7 through Fig. 9. Overall, the Southern Alaska region has the highest wave resource within the EEZ domain, followed by the West Coast and Hawaii regions (Figs. 7 and 8). The GoM region has the least wave energy among all the regions and the East Coast region shows strong spatial gradient across the shore (Figs. 7 and 8). The southern portion of the Southern Alaska region shows a greater energy resource than the northern portion because of the sheltering effect of the Aleutian Islands (Fig. 8). Similarly, wave energy in northeastern region of Hawaii is also greater than that in the southwestern region because of the sheltering effect of the Hawaii islands. Also, there is significant latitudinal variability in the wave resource in the West and East Coast regions, as discussed by Yang et al. (2020) [56] and Ahn et al. (2021) [73], respectively. Wave energy periods in the Pacific Ocean are much longer that those in the Atlantic Ocean (Fig. 9). The West Coast region has the longest wave period because of the longest fetch, which is consistent with the results shown in the aggregation analysis (Tables 7 and 8). The GoM region also has the shortest wave period, mostly between 3 and 6 s, because of the fetch being limited in a semi-enclosed basin.

The IEC-TS 62600–101 also recommends bivariate analysis based on the time series distribution of wave height and wave period as part of the resource characterization. For this purpose, we generated the bivariate distribution at selected locations in each other region. To achieve a consistent evaluation, all stations selected are 2 km from shore and facing the open ocean. The selected stations are not shallow enough for depth-induced breaking to be active, thereby acting as an upper limit in the distributions. Fig. 10 shows the bivariate distributions at selected stations in each region. While all the panels have the same x- (T_e) and y-axes scales (H_{m0}), to emphasize the distributions at each station rather than comparing magnitudes among all the stations the color scale for the probability distribution is not constant across panels. The station in American Samoa is on the east shore of the island, partially sheltered from the northwestern swells that are active in the boreal winter [66]. However, it is exposed to the southwestern swells (~1.5–2.5 m), which have fairly long periods (~9 s) (Fig. 10a). The station in Guam shows a wave climate similar to that of American Samoa but with a shorter wave period and smaller wave height (Fig. 10b). The northeast shore of Hawaii experiences waves whose heights are mostly in the range of 1.5–2.5 m and wave periods are longer than 7 s (Fig. 10c). A station south of the Aleutian Islands in Alaska experiences a broad range of wave heights, from 1 m to more than 6 m and a wave period mostly in the range of 7–11 s (Fig. 10d), representing complex and energetic sea states in Alaska. The Washington coast also experiences a wide range of wave heights and periods; most occurrences are in the 1.5–3.5 m and 8–12 s range, but the tail of the significant wave height can reach more than 6.5 m (Fig. 10e). This is consistent with the large-scale assessment of increasing wave period eastward in the north Pacific [71]. Wave climate in the GoM region features small wave heights (<1.5 m) and short-wave periods (<7 s) (Fig. 10f). However, the tail of significant wave height can reach up to 6.5 m as a result of hurricanes. In the Gulf of Maine on the East Coast, waves are also mostly in the range of <2.5 m in wave height and <7 s in wave period. However, the tail of the wave climate is widespread in both wave height (up to 6.5 m) and energy period (up to 13 s) (Fig. 10g). The northern shore of Puerto Rico is exposed to the Atlantic Ocean and receives the longest period waves in PRUSVI (Fig. 10h). The tail of the significant wave height distributions extends to higher waves in the GoM and East Coast regions, presumably because of longer uninterrupted fetches of tropical storms and hurricanes, but further research into the variability of these extreme

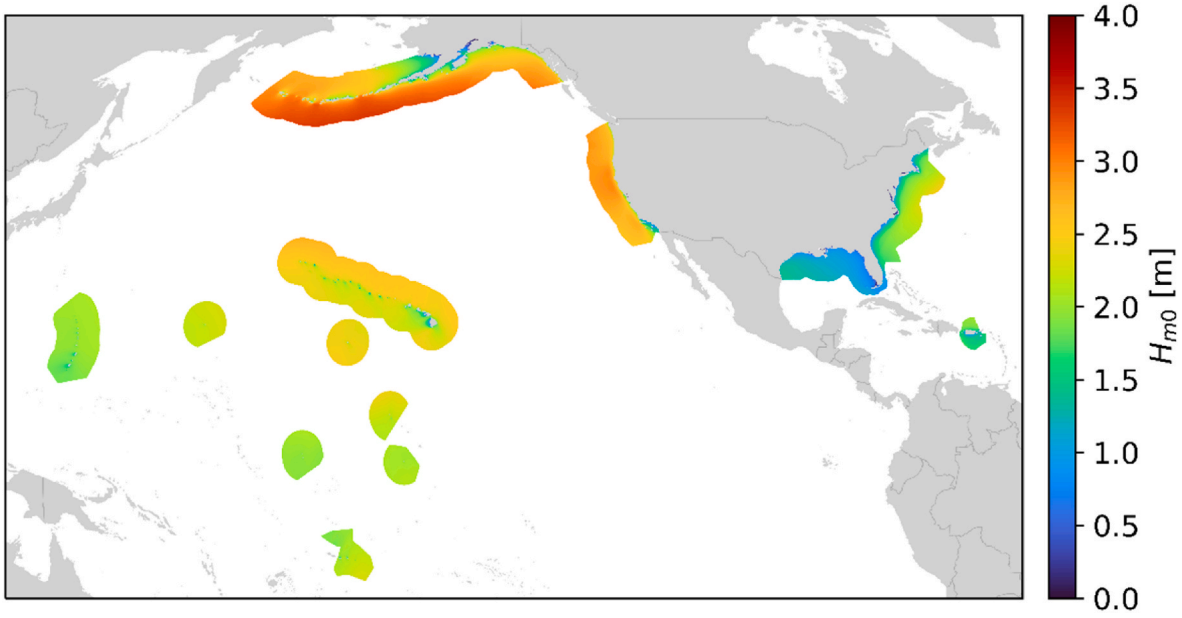

Fig. 7. Simulated 42-year averaged significant wave height for the U.S. EEZ in the Pacific and Atlantic regions.

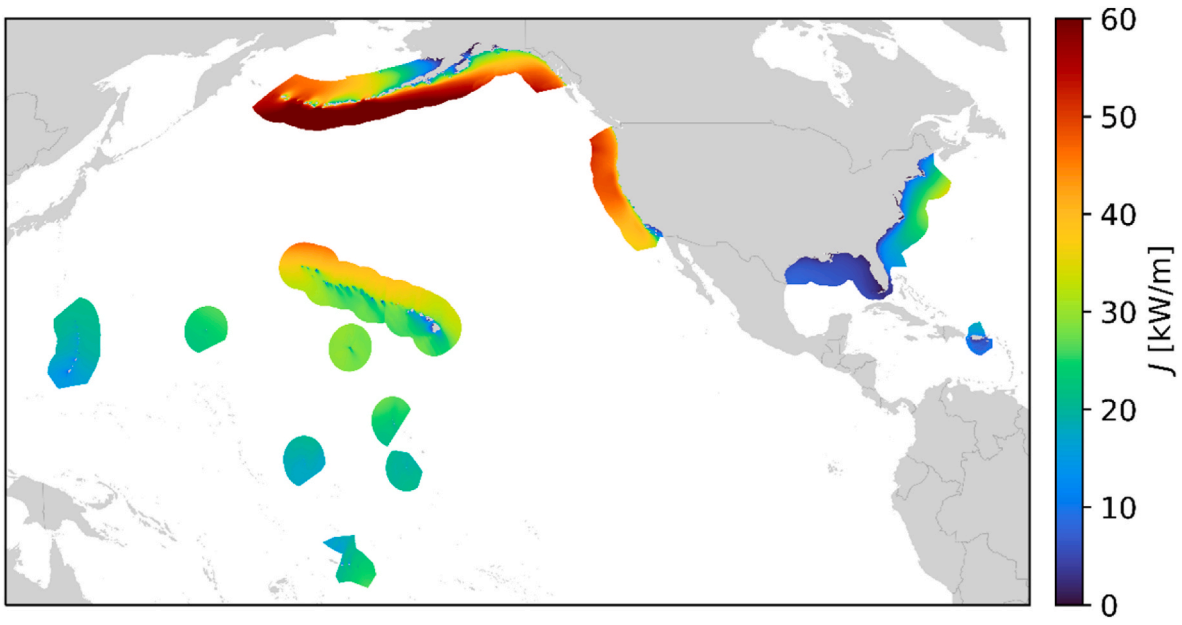

Fig. 8. Simulated 42-year omnidirectional wave power for the U.S. EEZ in the Pacific and Atlantic regions.

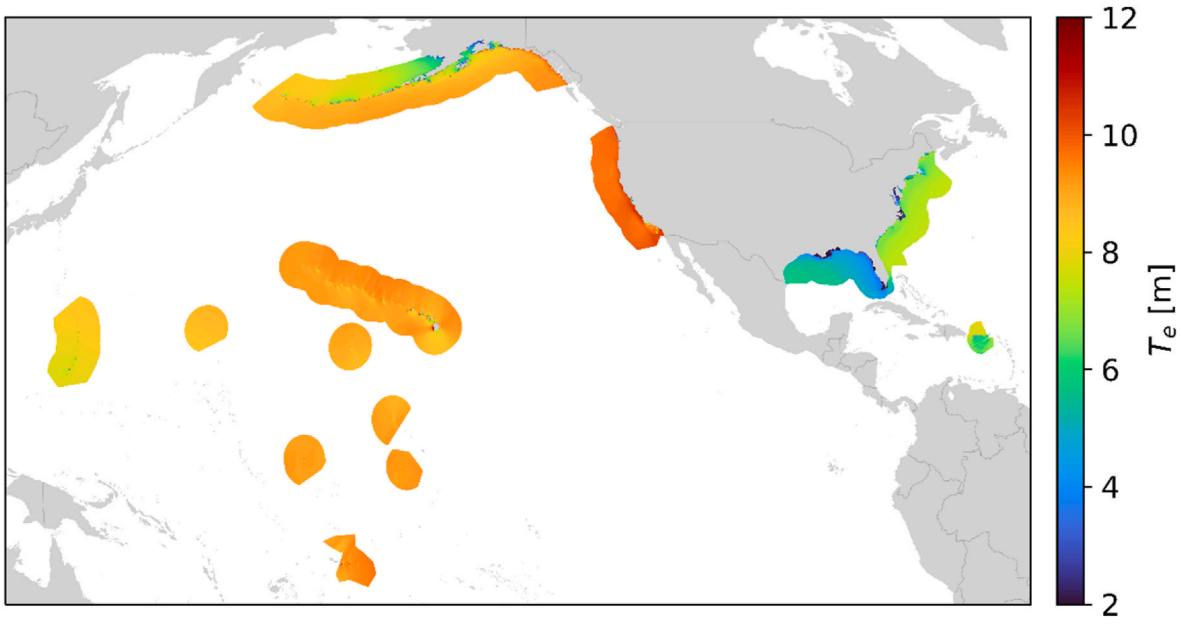

Fig. 9. Simulated 42-year averaged wave energy period for the U.S. EEZ in the Pacific and Atlantic regions.

parameters is needed.

4.3. Temporal variability of wave resource

The monthly variabilities of wave power at 2 km from shore and along the 100 m isobath in each region are shown in Figs. 11 and 12, respectively. In general, regions in the Atlantic Ocean have less monthly variability than those in the Pacific Ocean, especially at stations 2 km from shore. The West Coast region has the largest monthly variability among all the regions at 2 km from shore and along the 100 m isobath, while the GoM region has the smallest wave resource but also experiences the least monthly variability in both cases compared to the rest of the regions (Figs. 11 and 12). All regions, except USPT, show the lowest wave resource in the summer months 2 km from shore (Fig. 11). The small peak in wave power observed in July–September in the USPT region is mainly due to the exposure of American Samoa to the Southern Ocean swells, which intensify during the austral winter [66]. Winter (boreal) is the most energetic period (December and January) and shows the highest wave energy in all regions except the GoM, where most of the wave resource is locally generated, and February through April have the largest winds (Fig. 11). Therefore, the GoM region experiences peak wave energy during the months of February to April. The GoM also experiences the smallest wave energy from July to September even when influenced by hurricanes (Fig. 11). Of all the regions, the East Coast region has the second smallest wave resource and monthly variability at 2 km from shore, but it exhibits the third highest wave energy as well as monthly variability in the winter along the 100 m isobath, after the West Coast and Southern Alaska regions (Fig. 12).

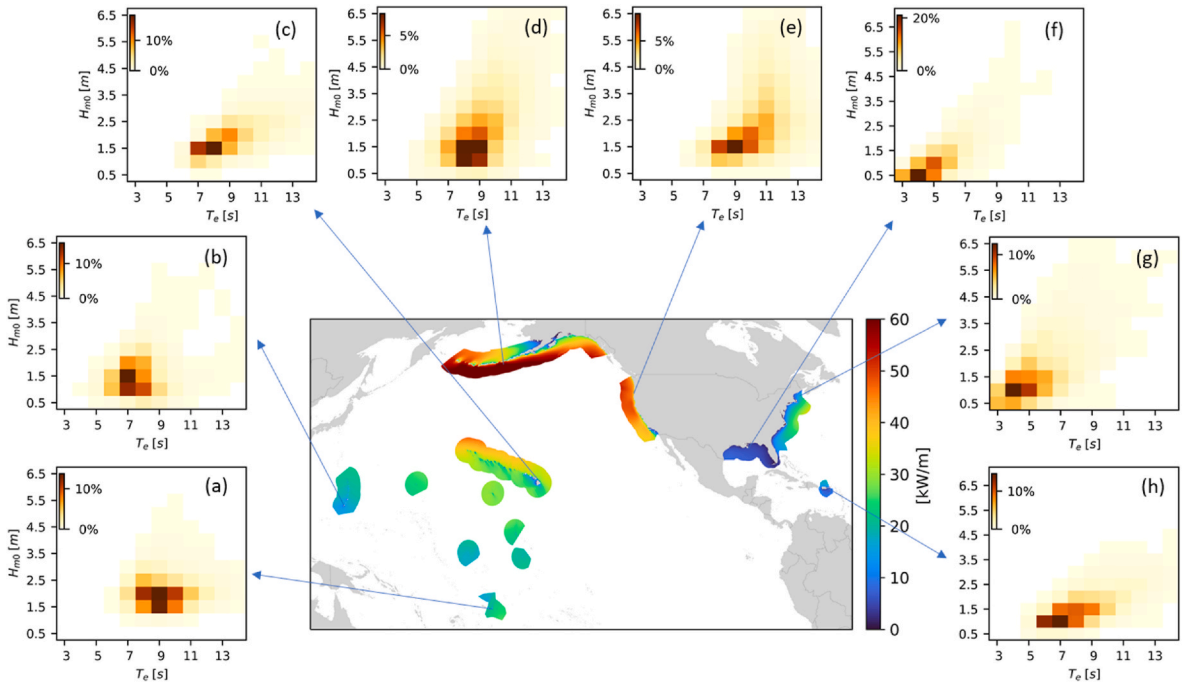

Fig. 10. 42-year averaged wave climate based on the bivariate distribution of significant wave height and energy period in (a) American Samoa, (b) Guam and the Commonwealth of the Northern Mariana Islands, (c) Hawaii, (d) Aleutian Islands of Alaska, (e) Northern Washington on the West Coast, (f) Gulf of Maine on the East Coast, (g) Mississippi River Delta of the GoM, and (h) Puerto Rico. The center image shows the 42-year averaged omnidirectional wave power.

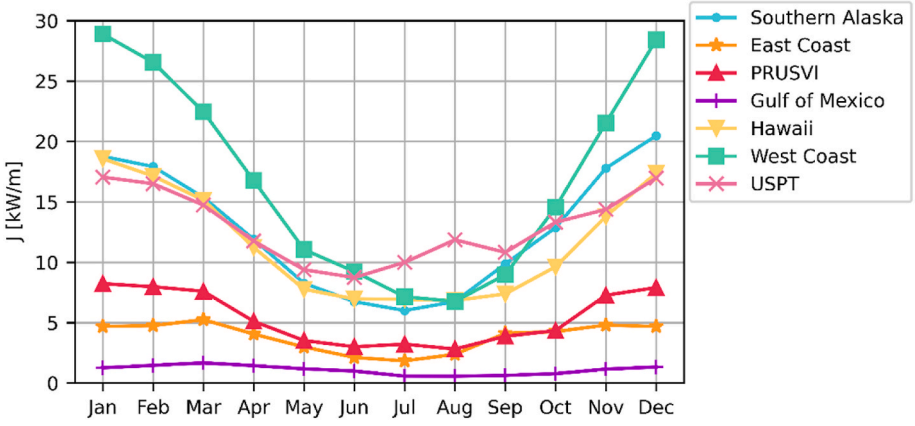

Fig. 11. Comparison of the monthly variability of omnidirectional wave power at 2 km offshore for different regions.

5. Data dissemination

The wave resource hindcast datasets, which include 42-year 3-h time series of the six IEC resource statistics at all model grid points and thousands of virtual buoy sites with hourly two-dimensional wave spectra, are hosted on the Amazon Web Services (AWS) Registry of Open Data (https://registry.opendata.aws/wpto-pds-us-wave/), a database maintained by NREL. The full datasets have several hundred terabytes of data organized into a collection of. h5 files, ranging from 2.5 to 455.2 gigabytes in size. Hosting the hindcast datasets on the AWS database ensures that the data are publicly available and allows users to access each dataset in its entirety or derive a subset of it using a variety of approaches. The goal of the AWS open-source database is to disseminate the wave resource data to designers of WEC technologies and WEC project developers, and to promote further research not only on the characterization and assessment of U.S. wave energy resources, but also on the effect of climate change on nearshore wave climate, extreme sea state and operational safety, coastal hazards, and community resilience.

The hindcast datasets are also disseminated through the Marine Energy Atlas (https://maps.nrel.gov/marine-energy-atlas/), where users can visualize variables of interest for particular locations, and have the option to spatially or temporally subset the data for download. Users can also download subsets of data through their web browser by navigating through the AWS Registry of Open Data to the region and then the year of interest (https://data.openei.org/s3_viewer?bucket=wpto-pds-us-wave&prefix=v1.0.0%2F).

The datasets can also be accessed using the Marine and Hydrokinetic Toolkit (MHKiT) software (https://github.com/MHKiT-Software) or directly from the database on AWS. MHKiT is software that can be run through Python and MATLAB, and it includes tools that enable users to analyze and explore data. The Wave Module within MHKiT contains functions to download and analyze the dataset, and it includes access to complementary data and tools for streamlined analytical and processing workflows. Through the AWS command line interface (https://aws.amazon.com/cli/), users can download the entire dataset to their local machine, but this requires significant data storage volume. Details about

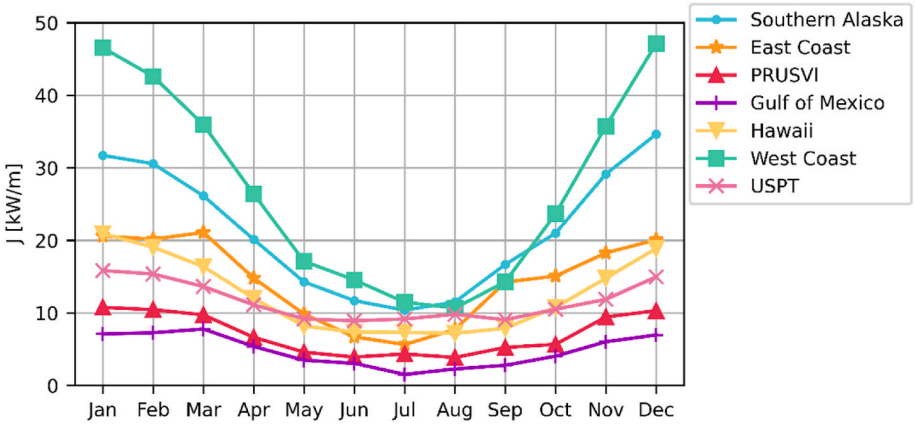

Fig. 12. Comparison of the monthly variability of omnidirectional wave power at the 100 m water depth for different regions. Note that the Y scale is different from Fig. 11.

accessing the dataset can be found here: https://www.nrel.gov/water/wave-hindcast-dataset.html.

6. Summary and conclusions

This study presents the 42-year regional wave hindcast datasets for the US EEZs using high-resolution SWAN models and the national-scale wave resource characterization based on the hindcast datasets. Aggregated statistics of wave resources derived using the IEC-TS 62600-101 methodology showed that the wave resource is high and exhibits regional and significant monthly variability in different regions of the U. S. The wave hindcast models generate time series for a variety of wave energy resource statistics, including wave power at a 200 m resolution up to 30 km off the coastline, depending on the regional characteristics. These statistics facilitate high-fidelity characterization, classification, and assessment of the U.S. wave energy resources, including assessment of wave energy project opportunities, constraints, and risks. Because the regional models cover the entire U.S. EEZs, the hindcast datasets can also be used to provide wave boundary conditions for local studies for design class assessments [10].

The regional hindcast models were extensively validated for wave resource parameters using wave buoy measurements and altimetry data. Overall, the regional wave models showed good agreement with observations obtained from wave buoy data and altimetry data. Relatively speaking, error statistics are generally larger in the Southern Alaska, East Coast, and GoM regions, which are subject to extreme weather events such as extratropical storms and hurricanes, indicating the need for model improvement in simulating large waves in extreme sea states.

Wave resource characterization was conducted for all the coastal regions in the U.S. based on hindcast data sampled at 2 km from shore and along the 100 m isobath. Aggregations of resource parameters and regional distributions of wave resources showed that the West Coast region has the highest resource and monthly variability, while the GoM region has the lowest wave power and monthly variability at 2 km from shore and along 100 m isobath. Significant wave resources exist in the East Coast region along the 100 m isobath, and they have the potential for deep water wave harvesting in support of Power Blue Economy (PBE) applications, such as offshore ocean observation systems.

While support of wave energy research and development drove the development of these datasets, they are also valuable for other coastal applications such as the offshore wind energy industry, coastal and ocean planning, coastal engineering, and coastal resilience. The datasets also have potential use for evaluating historical nonstationary wave climate trends and interannual variability due to climate change, PBE, and coastal resilience.

Model errors due to limitations of physics packages in the model and errors of wind forcing will affect the accuracy of wave resource estimates, especially for large waves during extreme events. For example, underpredicting or overpredicting of wave power will result in under- or over-estimates of the wave resource. It is important to update the hindcasts when new physics packages and more accurate wind products become available.

Although the regional hindcasts were validated and provide valuable long-term, high-resolution wave datasets to support WEC development and other coastal ocean applications, limitations in the models warrant future research. For example, the current hindcasts do not cover the northern Alaska region—the Bering Sea and the Alaskan Artic Coast—because of the challenge of simulating effects of sea-ice on waves. In recent developments and research related to sea-ice effects in wave modeling [34,74–76], it is now possible to extend the Alaska region to cover the entire EEZ in Alaska. Wind is the most important forcing for wave hindcast and forecast modeling, so it is important to incorporate new wind product with higher resolution in wave hindcasts when possible. Future research on long-term decadal variability [56,77] and the effect of climate change on wave resource in different regions should be also considered. This present study did not consider ocean current forcing and wave-current interaction because in most of the nearshore regions the effect is small. However, the East Coast region shows good wave resources farther offshore where wave interaction with the Gulf Stream could play an important role in wave power [78–80]. Cook Inlet, a large semi-enclosed bay in Alaska, represents the highest tidal stream energy potential with strong tidal current in the U.S., and wave-current coupling modeling should be considered to improve both wave and tidal current predictions [81]. Furthermore, additional statistics on extreme wave conditions to characterize wave loads for WEC design should also be considered in future study.

CRediT authorship contribution statement

Zhaoqing Yang: Conceptualization, Methodology, Investigation, Formal analysis, Supervision, Project administration, Funding acquisition, Writing - original draft, Writing - review & editing. **Gabriel García Medina:** Conceptualization, Methodology, Investigation, Formal analysis, Writing – original draft, Writing – review & editing, Visualization. **Vincent S. Neary:** Conceptualization, Methodology, Investigation, Writing – review & editing, Supervision, Project administration, Funding acquisition. **Seongho Ahn:** Conceptualization, Methodology, Investigation, Formal analysis, Writing – review & editing, Visualization. **Levi Kilcher:** Writing – review & editing, Project administration, Funding acquisition. **Aidan Bharath:** Data Processing and Curation.

Declaration of competing interest

The authors declare that they have no known competing financial interests or personal relationships that could have appeared to influence the work reported in this paper.

Acknowledgments

This study was funded by the U.S. Department of Energy (DOE), Office of Energy Efficiency and Renewable Energy, Water Power Technologies Office. This work was authored in part by the Pacific Northwest National Laboratory, operated by Battelle Memorial Institute for the DOE's Office of Energy Efficiency & Renewable Energy (EERE) under contract DE-AC05-76RL01830; Sandia National Laboratories, a multimission laboratory managed and operated by National Technology and Engineering Solutions of Sandia, LLC., a wholly owned subsidiary of Honeywell International, Inc., for the DOE's National Nuclear Security Administration under contract DE-NA0003525; and National Renewable Energy Laboratory, operated by Alliance for Sustainable Energy, LLC for the DOE's Office of EERE, under Contract No. DE-AC36-08GO28308.

All model simulations and data processing were performed at high-performance computing facilities in DOE's national laboratories, including Constance at PNNL, Chama and Skybridge at Sandia, and Eagle at NREL.

Some of the wave data were furnished by the Coastal Data Information Program (CDIP), Integrative Oceanography Division, operated by the Scripps Institution of Oceanography, under the sponsorship of the U.S. Army Corps of Engineers and the California Department of Parks and Recreation. Bathymetry and wave measurements in the USPT and Hawaii regions were provided by PacIOOS (www.pacioos.org), which is a part of the U.S. Integrated Ocean Observing System (IOOS®), funded in part by National Oceanic and Atmospheric Administration (NOAA) Awards #NA16NOS0120024 and #NA21NOS0120091. Additional buoy data were provided by the NOAA National Data Buoy Center and the Department of Fisheries and Ocean, Canada.

This paper describes objective technical results and analysis. The views expressed in the article do not necessarily represent the views of the DOE or the U.S. Government. The U.S. Government retains, and the publisher, by accepting the article for publication, acknowledges, that the U.S. Government retains a nonexclusive, paid-up, irrevocable, worldwide license to publish or reproduce the published form of this work, or allow others to do so, for U.S. Government purposes.

References

[1] A. Ribal, I.R. Young, 33 Years of Globally Calibrated Wave Height and Wind Speed Data Based on Altimeter Observations, vol. 6, Scientific Data, 2019, p. 6, 77, 2019.
[2] S. Ahn, V.S. Neary, K.A. Haas, Global wave energy resource classification system for regional energy planning and project development, Renew. Sustain. Energy Rev. vol. 162 (2022).
[3] A. Cornett, A global wave energy resource assessment, Sea Technol. 50 (4) (2009) 59–64.
[4] C.W. Zheng, Q. Wang, C.Y. Li, An overview of medium- to long-term predictions of global wave energy resources, Renewable Sustainable Energy Rev. 79 (2017) 1492–1502.
[5] Z. Yang, A. Copping, Marine Renewable Energy – Resource Characterization and Physical Effects, Springer International Publishing, 2017.
[6] T. Mai, et al., Renewable electricity futures for the United States, IEEE Trans. Sustain. Energy 5 (2) (2014) 372–378.
[7] G. Mork, et al., Assessing the global wave energy potential, in: Proceedings of the Asme 29th International Conference on Ocean, Offshore and Arctic Engineering 2010, vol. 3, 2010, pp. 447–454.
[8] M. Wiatros-Motyka, Global Electricity Mid-year Insights 2022, 2022.
[9] L. Kilcher, M.L. Fogarty, M., Marine Energy in the United States: an Overview of Opportunities, National Renewable Energy Laboratory, Golden, CO, 2021, p. 48.
[10] IEC, TS 62600 Marine Energy – Wave, Tidal and Other Water Current Converters – Part 101: Wave Energy Resource Assessment and Characterization, International Electrotechnical Commission, Geneva, Switzerland, 2015.
[11] EPRI, Mapping and assessment of the United States ocean wave energy resource, in: EPRI 2011 Technical Report to U.S. Department of Energy, Electric Power Research Institute, Palo Alto, California, 2011.
[12] G. García-Medina, H.T. Özkan-Haller, P. Ruggiero, Wave resource assessment in Oregon and southwest Washington, USA, Renew. Energy 64 (2014) 203–214.
[13] S. Ahn, K.A. Haas, V.S. Neary, Wave energy resource characterization and assessment for coastal waters of the United States, Appl. Energy (2020) 267.
[14] M.A. Hemer, et al., A revised assessment of Australia's national wave energy resource, Renew. Energy 114 (2017) 85–107.
[15] M.G. Hughes, A.D. Heap, National-scale wave energy resource assessment for Australia, Renew. Energy 35 (8) (2010) 1783–1791.
[16] P. Gleizon, et al., Wave energy resources along the European atlantic coast, in: Z.Y. a.A. Copping (Ed.), Marine Renewable Energy - Resource Characterization and Physical Effects, Springer, Switzerland, 2017, pp. 37–69.
[17] V.S. Kumar, T.R. Anoop, Wave energy resource assessment for the Indian shelf seas, Renew. Energy 76 (2015) 212–219.
[18] B. Liang, et al., 22-Year wave energy hindcast for the China East Adjacent Seas, Renew. Energy 71 (2014) 200–207.
[19] Z.F. Wang, C.L. Duan, S. Dong, Long-term wind and wave energy resource assessment in the South China sea based on 30-year hindcast data, Ocean Eng. 163 (2018) 58–75.
[20] K. Sasmal, et al., Assessment of wave energy resources and their associated uncertainties for two coastal areas in Japan, J. Mar. Sci. Technol. 26 (3) (2021) 917–930.
[21] A. Webb, T. Waseda, K. Kiyomatsu, A high-resolution, long-term wave resource assessment of Japan with wave-current effects, Renew. Energy 161 (2020) 1341–1358.
[22] M. Goncalves, P. Martinho, C.G. Soares, Wave energy conditions in the western French coast, Renew. Energy 62 (2014) 155–163.
[23] J.P. Sierra, et al., Assessment of the intra-annual and inter-annual variability of the wave energy resource in the Bay of Biscay (France), Energy 141 (2017) 853–868.
[24] S.P. Neill, et al., Inter-annual and inter-seasonal variability of the Orkney wave power resource, Appl. Energy 132 (2014) 339–348.
[25] S.P. Neill, et al., The wave and tidal resource of Scotland, Renew. Energy 114 (2017) 3–17.
[26] R.P.G. Mendes, M.R.A. Calado, S.J.P.S. Mariano, Wave energy potential in Portugal-Assessment based on probabilistic description of ocean waves parameters, Renew. Energy 47 (2012) 1–8.
[27] D. Silva, P. Martinho, C.G. Soares, Wave energy distribution along the Portuguese continental coast based on a thirty three years hindcast, Renew. Energy 127 (2018) 1064–1075.
[28] L. Liberti, A. Carillo, G. Sannino, Wave energy resource assessment in the Mediterranean, the Italian perspective, Renew. Energy 50 (2013) 938–949.
[29] M. Monteforte, C. Lo Re, G.B. Ferreri, Wave energy assessment in Sicily (Italy), Renew. Energy 78 (2015) 276–287.
[30] F. Salimi, C. Ershadi, V. Chegini, Forty years wind wave power assessment in the high-energy region of Persian Gulf, Int. J. Environ. Sci. Technol. 19 (4) (2022) 2677–2702.
[31] L. Rusu, E. Rusu, Evaluation of the worldwide wave energy distribution based on ERA5 data and altimeter measurements, Energies 14 (2) (2021).
[32] B.G. Reguero, I.J. Losada, F.J. Mendez, A global wave power resource and its seasonal, interannual and long-term variability, Appl. Energy 148 (2015) 366–380.
[33] G. García-Medina, et al., Wave resource characterization at regional and nearshore scales for the US Alaska coast based on a 32-year high-resolution hindcast, Renew. Energy 170 (2021) 595–612.
[34] R. Branch, et al., Modeling Sea ice effects for wave energy resource assessments, Energies 14 (12) (2021).
[35] M.N. Allahdadi, et al., Development and calibration of a high-resolution model for the Gulf of Mexico, Puerto Rico, and the US Virgin Islands: implication for wave energy resource characterization, Ocean Eng. (2021) 235.
[36] M.N. Allahdadi, et al., Development and validation of a regional-scale high-resolution unstructured model for wave energy resource characterization along the US East Coast, Renew. Energy 136 (2019) 500–511.
[37] WAMDI, The WAM model - a third generation ocean wave prediction model, J. Phys. Oceanogr. 18 (12) (1988).
[38] H.L. Tolman, A 3rd-generation model for wind-waves on slowly varying, unsteady, and inhomogeneous depths and currents, J. Phys. Oceanogr. 21 (6) (1991) 782–797.
[39] H.L. Tolman, A new global wave forecast system at NCEP, Ocean Wave Meas. Anal. 1 and 2 (1998) 777–786.
[40] N. Booij, R.C. Ris, L.H. Holthuijsen, A third-generation wave model for coastal regions - 1. Model description and validation, J. Geophys. Res. Oceans 104 (C4) (1999) 7649–7666.
[41] R.C. Ris, L.H. Holthuijsen, N. Booij, A third-generation wave model for coastal regions - 2. Verification, J. Geophys. Res. Oceans 104 (C4) (1999) 7667–7681.
[42] M. Benoit, F. Marcos, F. Becq, *TOMAWAC: a prediction model for offshore and nearshore storm waves.* Environmental and Coastal Hydraulics: protecting the Aquatic Habitat, Proc. Theme B 1 & 2 (27) (1997) 1316–1321.
[43] DHI, Mike 21 Spectral Waves FM - Short Description, DHI: Horsholm Denmark, 2012, p. 16.
[44] SWAN, SWAN: User Manual, Cycle III Version 41.01A, Delft University of Technology, Delft, The Netherlands, 2015.
[45] S. Hasselmann, et al., Computations and parameterizations of the nonlinear energy-transfer in a gravity-wave spectrum .2. Parameterizations of the nonlinear energy-transfer for application in wave models, J. Phys. Oceanogr. 15 (11) (1985) 1378–1391.
[46] J.A. Battjes, J.P.F.M. Janssen, Energy loss and set-up due to breaking random waves, in: 16th Conference on Coastal Engineering, ASCE, Hamburg, Germany, 1978.

[47] L. Cavaleri, P.M. Rizzoli, Wind wave prediction in shallow-water - theory and applications, J. Geophys. Res. Ocean Atmos. 86 (Nc11) (1981) 961–973.
[48] G.J. Komen, S. Hasselmann, K. Hasselmann, On the existence of a fully-developed wind-sea spectrum, J. Phys. Oceanogr. 14 (8) (1984) 1271–1285.
[49] A. Chawla, D.M. Spindler, H.L. Tolman, Validation of a thirty year wave hindcast using the Climate Forecast System Reanalysis winds, Ocean Model. 70 (2013) 189–206.
[50] S. Saha, et al., The ncep climate forecast system reanalysis, Bull. Am. Meteorol. Soc. 91 (8) (2010) 1015–1057.
[51] S. Saha, et al., The NCEP climate forecast system version 2, J. Clim. 27 (6) (2014) 2185–2208.
[52] W.C. Skamarock, J.B. Klemp, A time-split nonhydrostatic atmospheric model for weather research and forecasting applications, J. Comput. Phys. 227 (7) (2008) 3465–3485.
[53] J.E. Stopa, K.F. Cheung, Intercomparison of wind and wave data from the ECMWF reanalysis interim and the NCEP climate forecast system reanalysis, Ocean Model. 75 (2014) 65–83.
[54] Y. Eldeberky, Nonlinear transformation of wave spectra in the nearshore zone (Ph. D. Thesis), in: Department of Civil Engineering, Delft University of Technology, Netherlands, 1996.
[55] W.C. Wu, et al., Development and validation of a high-resolution regional wave hindcast model for U.S. West Coast wave resource characterization, Renew. Energy 152 (2020) 736–753.
[56] Z.Q. Yang, et al., Characteristics and variability of the nearshore wave resource on the US West Coast, Energy (2020) 203.
[57] T. Wang, et al., A high-resolution regional wave resource Characterization for the U.S. West coast, in: Offshore Technology Conference, 2020. Houston, USA.
[58] M. Zijlema, Computation of wind-wave spectra in coastal waters with SWAN on unstructured grids, Coast. Eng. 57 (3) (2010) 267–277.
[59] P.A.E.M. Janssen, Quasi-linear theory of wind-wave generation applied to wave forecasting, J. Phys. Oceanogr. 21 (11) (1991) 1631–1642.
[60] K. Hasselmann, et al., Measurements of wind-wave growth and swell decay during the joint north sea wave project (JONSWAP), Ergaenzungsheft Zur Deutschen Hydrographischen Zeitschrift (1973) 95.
[61] L. Rusu, The wave and wind power potential in the western Black Sea, Renew. Energy 139 (2019) 1146–1158.
[62] J.A. Bowers, I.D. Morton, G.I. Mould, Directional statistics of the wind and waves, Appl. Ocean Res. 22 (1) (2000) 13–30.
[63] J.L. Hanson, et al., Pacific hindcast performance of three numerical wave models, J. Atmos. Ocean. Technol. 26 (8) (2009) 1614–1633.
[64] N. Li, et al., Wave energy resources assessment for the multi-modal sea state of Hawaii, Renew. Energy 174 (2021) 1036–1055.
[65] N. Li, et al., Wave climate and energy resources in the Mariana Islands from a 42-year high-resolution hindcast, Renew. Energy (2023) (in revision).
[66] G. García-Medina, et al., Wave climate and energy resources in American Samoa from a 42-year hindcast, Renew. Energy (2023). https://doi.org/10.1016/j.renene.2023.03.031.
[67] S. Ahn, et al., A framework for feasibility-level validation of high-resolution wave hindcast models, Ocean Eng. (2022) 263.
[68] S. Zieger, J. Vinoth, I.R. Young, Joint calibration of multiplatform altimeter measurements of wind speed and wave height over the past 20 years, J. Atmos. Ocean. Technol. 26 (12) (2009) 2549–2564.
[69] N. Li, et al., Thirty-four years of Hawaii wave hindcast from downscaling of climate forecast system reanalysis, Ocean Model. 100 (2016) 78–95.
[70] D.B. Chelton, et al., in: L.-L. Fu, A. Cazenave (Eds.), Satellite Altimetry. Satellite Altimetry and Earth Sciences: A Handbook of Techniques and Applications, Acadenuc Press, 2021, p. 131.
[71] R.A. Arinaga, K.F. Cheung, Atlas of global wave energy from 10 years of reanalysis and hindcast data, Renew. Energy 39 (1) (2012) 49–64.
[72] E.K.M. Chang, Y.F. Fu, Interdecadal variations in Northern Hemisphere winter storm track intensity, J. Clim. 15 (6) (2002) 642–658.
[73] S. Ahn, et al., Nearshore wave energy resource characterization along the East Coast of the United States, Renew. Energy 172 (2021) 1212–1224.
[74] V.T. Cooper, et al., Wind waves in sea ice of the western Arctic and a global coupled wave-ice model, Phil. Trans. Math. Phys. Eng. Sci. 380 (2235) (2022).
[75] S. Iwasaki, J. Otsuka, Evaluation of wave-ice parameterization models in WAVEWATCH III (R) along the coastal area of the sea of okhotsk during winter, Front. Mar. Sci. 8 (2021).
[76] K. Nederhoff, et al., The effect of changing sea ice on wave climate trends along Alaska's central Beaufort Sea coast, Cryosphere 16 (5) (2022) 1609–1629.
[77] S. Ahn, V.S. Neary, Non-stationary historical trends in wave energy climate for coastal waters of the United States, Ocean Eng. 216 (2020), 108044.
[78] C.A. Hegermiller, et al., Wave-current interaction between hurricane matthew wave fields and the Gulf stream, J. Phys. Oceanogr. 49 (11) (2019) 2883–2900.
[79] Y.J. Sun, W. Perrie, B. Toulany, Simulation of wave-current interactions under hurricane conditions using an unstructured-grid model: impacts on ocean waves, J. Geophys. Res. Oceans 123 (5) (2018) 3739–3760.
[80] D.W. Wang, et al., Wave-current interaction near the gulf-stream during the surface-wave dynamics experiment, J. Geophys. Res. Oceans 99 (C3) (1994) 5065–5079.
[81] T.P. Wang, Z.Q. Yang, A tidal hydrodynamic model for cook inlet, Alaska, to support tidal energy resource characterization, J. Mar. Sci. Eng. 8 (4) (2020).